Influence of Steric Confinement within Zeolite Y on Photoinduced Energy Transfer between $[Ru(bpy)_3]^{2+}$ and Iron Polypyridyl Complexes

Gavin Sewell, Robert J. Forster, and Tia E. Keyes*

School of Chemical Sciences, National Centre for Sensor Research, Dublin City University, Glasnevin, Dublin 9, Ireland

Received: September 19, 2007; In Final Form: November 5, 2007

The spectroscopic and photophysical properties of zeolite-Y-entrapped $[Ru(bpy)_3]^{2+}$ co-doped with either $[Fe(bpy)_3]^{2+}$ or $[Fe(tpy)_2]^{2+}$ over a range of iron complex loadings are presented. In solution, $[Ru(bpy)_3]^{2+}$ undergoes efficient bimolecular energy transfer to $[Fe(bpy)_3]^{2+}$, whereas only radiative or trivial energy transfer occurs between $[Ru(bpy)_3]^{2+}$ and $[Fe(tpy)_2]^{2+}$. In sharp contrast, within zeolite Y, both $[Fe(bpy)_3]^{2+}$ and $[Fe(tpy)_2]^{2+}$ were found to effectively quench the donor emission. Fitting the Perrin model to the photophysical data yields an effective quenching radius of 32 and 27 Å, respectively, for $[Fe(bpy)_3]^{2+}$ and $[Fe(tpy)_2]^{2+}$. The long-range nature of the quenching suggests Förster energy transfer. Detailed spectroscopic investigations indicate that $[Fe(tpy)_2]^{2+}$ bound within zeolite Y undergoes significant distortion from octahedral geometry. This distortion results in increased oscillator strength and enhanced spectral overlap, between the $[Ru(bpy)_3]^{2+}$ $^3d\pi-\pi^*$ donor emission and the co-incident acceptor $^1T2-{}^1A1$ ligand field absorption compared with solution. This turns on an efficient energy transfer to $[Fe(tpy)_2]^{2+}$ within the confinement of the zeolite Y supercage. Overall, this is an interesting example of the ability of the zeolite environment to provoke new photophysical processes not possible in solution.

Introduction

Organization and confinement of donor and acceptor species in three-dimensional space is a key challenge in supramolecular chemistry if practical applications are to be developed. Strategies for generating condensed phase assemblies capable of photo- or electrochemically addressable functions have included assembly of photo- and electroactive species at interfaces,[1,2] crystal engineering,[3] and the incorporation of electrochemically/optically active components into solid matrices such as sol gel,[4,5] zeolite,[6] and other mesoporous substrates.[7,8]

The particular advantages of zeolites are their optical transparency, their relative chemical inertness, and their highly regular cavities and channels.[9] Zeolite Y has proven particularly interesting because of its relatively large pore size. It possesses a three-dimensional network of approximately spherical supercages of about 1.3 nm in diameter connected tetrahedrally through 0.74 nm windows. Since the pore diameter exceeds the entry aperture, reagents can be introduced through the aperture and reacted in situ in the pore to produce products that are too large to escape the zeolite without its destruction. This "ship in a bottle" approach has led to a number of interesting photophysical studies of both organic and inorganic fluorophores which are translationally trapped in the zeolite.[10] Indeed, the pore environment has been demonstrated to provoke changes in the photochemistry and photophysics of the guest, due to factors such as steric confinement and the dielectric properties of the aluminosilicate cage.[9,10]

The entrapment of long-lived luminophores such as $[Ru(bpy)_3]^{2+}$ in zeolite has attracted particular attention because of the potential importance of this species in applications such as solar energy conversion, photochemical molecular devices and sensing. Consequently $[Ru(bpy)_3]^{2+}$ entrapped in zeolite Y has been well studied, including the ability of this material to quantitatively sense O_2.[11,12]

Inter-supercage communication, both electron and energy transfer, has also been investigated. For example a number of elegant studies focused on ion exchanged donor-acceptors where reaction occurs at the surface of the zeolite and there is no encapsulation,[13,14] or materials in which $[Ru(bpy)_3]^{2+}$ is entrapped, but the donor or acceptor pair is small and diffuses freely through the zeolite.[15,16]

Relatively few studies have been made of donor acceptor systems in zeolite Y where both donor and acceptor species are nondiffusing. Notable exceptions include studies by Kincaid et al. where co-encapsulation of two ruthenium polypyridyl complexes were studied with appropriate thermodynamic properties so that once one complex is photooxidised by viologen exchanged into the zeolite, the second undergoes an interpore electron transfer.[17,18] In addition, Calzaferri and co-workers have reported on an elegant entrapment strategy whereby the channular structure of zeolite L can be plugged by donor or acceptor following ion exchange of donor or acceptor pair into the aluminosilicate.[19,20,21]

In this contribution, we describe the synthesis of the luminophore $[Ru(bpy)_3]^{2+}$ co-encapsulated with energy transfer acceptors $[Fe(bpy)_3]^{2+}$ and $[Fe(tpy)_2]^{2+}$ in zeolite Y. Here the donor and acceptor are prepared by ship in a bottle synthesis and are therefore both translationally trapped. The photophysical properties of $[Ru(tpy)_2]^{2+}$ in zeolite Y have been reported and demonstrated to be strongly impacted by entrapment.[22] We were interested to see how incorporation of the iron analogue was affected by zeolite encapsulation and whether this impacted on its interaction with the excited-state of $[Ru(bpy)_3]^{2+}$. The electronic properties of these co-encapsulates are presented, and detailed photophysical measurements suggest that, unlike the

* To whom correspondence should be addressed. E-mail: tia.keyes@dcu.ie.

10.1021/jp077542o CCC: $40.75
Published on Web 01/10/2008

reactants in solution, Förster energy transfer occurs between the excited-state donor and iron acceptor. The size of the metal complexes excludes the possibility for dynamic quenching process, and the rates and mechanism of this process are compared with analogous solution studies. Our studies indicate that steric confinement significantly affects the ability of the iron complex to quench the ruthenium excited state.

Experimental Section

Physical Measurements. Diffuse reflectance UV−vis experiments were conducted using either an Ocean Optics UV−vis spectrometer with diffuse reflectance angled fiber attachment or a Perkin-Elmer UV−vis NIR 900 spectrometer with a Spectralon coated integrating sphere. Na−Y zeolite was used as a blank, and spectra were recorded in absorbance mode. Luminescence spectra were collected using the Varian Cary Eclipse spectrofluorimeter employing a solid sample attachment for zeolite samples, undoped calcined Na−Y zeolite was used as a blank. All steady state and time-resolved measurements were carried out under ambient conditions. Luminescent lifetimes were determined from time-correlated single-photon-counting (TCSPC) using an Edinburgh Analytical instruments system (nF900 flash lamp and S900 detection system). The excitation pulse was generated by nitrogen discharge, pulsed at 40 kHz and monochromated to 337 nm. The temporal measurement window was typically ten times the longest-lived component. For the lifetime measurements, a small quantity of the zeolite material was dispersed in air equilibrated deionized water. After the experiment, the solution was filtered to confirm no residual luminescence was observed; that is, luminescence originates only from encapsulated species.

Raman spectroscopy was conducted using a confocal high-resolution Horiba Labram system. The exciting Ar ion laser (514 nm, 488 nm or 457. 9 nm) or diode laser (785 nm) was focused into the solution cell or onto a solid sample using a 10× objective lens. A spectral resolution of 0.1 cm^{-1} per pixel was achieved using a grating of 1800 lines/mm, and the *x* axis was calibrated against acetonitrile and silicon.

Materials. Hexaammineruthenium(III) chloride, 2,2′-bipyridine, 2,2′:6′,2″-terpyridine, iron(II) chloride-4-hydrate, ammonium iron(II) sulfate-6-hydrate, potassium hexafluorophosphate, hydrofluoric acid, hydrochloric acid, and all solvents were purchased from Sigma Aldrich and used without further purification.

Sodium zeolite Y was purchased from Sigma Aldrich and calcined in air at 600 °C for 6 h, extensively washed with 10% NaCl solution, and finally washed with deionized water until no chloride could be detected with silver nitrate solution (0.1 M).

Preparation of the Zeolite Encapsulated $[Ru(bpy)_3]^{2+}$ (Z-$[Ru(bpy)_3]^{2+}$). Z-$[Ru(bpy)_3]^{2+}$ was prepared using a method adapted from the work of Lundsford et al. and Bossmann et al., employing $[Ru(NH_3)_6]^{3+}$ as the precursor.[23,24] All solutions and suspensions were degassed with nitrogen and all procedures were performed under a nitrogen atmosphere in order to prevent formation of ruthenium red. Calcined Na−Y zeolite (11.91 g) was suspended in cold degassed deionized water (500 mL) at room temperature. The pH of this suspension was adjusted to pH 5.4 ± 0.1 using HCl (0.1 M). For an occupation of one ruthenium complex per 20 supercages, $[Ru(NH_3)_6]Cl_3$ (0.0851 g) was added to the solution, and this was stirred for 8 h at 4 °C. The resulting Z-$[Ru(NH_3)_6]^{3+}$ was filtered and washed with deionized water until no Cl^- could be detected using silver nitrate solution (0.1 M). The Z-$[Ru(NH_3)_6]^{3+}$ was then dried in vacuo and dispersed in degassed ethylene glycol (150 mL), dimethylsulfoxide (1 mL), and H_2O (1 mL). 2,2′-Bipyridine (0.154 g, which represented approximately a 20% excess) was added, and the slurry brought to reflux with stirring under nitrogen for 4 h. The resulting orange product was filtered and sonicated with copious amounts of hot ethanol, then dispersed in NaCl (10%w/v, 500 mL), and stirred for 1 h in order to remove superficially or surface bound ruthenium species. Finally, the doped zeolite was washed extensively with deionized water until no chloride could be detected in the filtrate using silver nitrate (0.1 M). Finally, excess 2,2′-bipyridine was removed by Soxhlet extraction into ethanol.

Preparation of Zeolite Encapsulated $[Fe(bpy)_3]^{2+}$and $[Fe(tpy)_2]^{2+}$. Calcined Na−Y zeolite (5.001 g) was suspended in cold degassed deionized water (100 mL). The pH of this suspension was then adjusted to pH 5.3 ± 0.1 using HCl (0.1 M). For an occupation of one iron species per 20 supercages, $FeCl_2{\cdot}4H_2O$ (0.0229 g) was added to the suspension. The solution was then left for 8 h at 4 °C with stirring. The Z-Fe^{2+} was filtered and washed with deionized water until no Cl^- could be detected using silver nitrate solution (0.1 M). These materials were dispersed in ethanol and the ligand added in 20% excess of a 3:1 and 2:1 ligand to metal molar ratio of 2,2′-bipyridine (0.0649 g) and 2,2′:6′,2″-terpyridine (0.0646 g), respectively. The suspensions were refluxed with stirring for 4 h. The products were filtered and washed with copious amounts of hot ethanol. The Z-$[Fe(bpy)_3]^{2+}$ or Z-$[Fe(tpy)_2]^{2+}$ was then dispersed in NaCl (10%w/v, 500 mL) and stirred for 30 min in order to remove superficially surface bound iron species. Finally, the doped zeolites were washed with deionized water until no chloride could be detected using silver nitrate solution (0.1 M). Excess 2,2′-bipyridine and 2,2′:6′,2″-terpyridine were removed by further washing in hot ethanol.

The corresponding parent iron compounds $[Fe(bpy)_3][PF_6]_2$ and $[Fe(tpy)_2][PF_6]_2$ were prepared from ammonium iron(II) sulfate-6-hydrate and the appropriate ligands according to standard procedures.[25]

Preparation of Co-doped Zeolite Encapsulated Z-$[Ru(bpy)_3]^{2+}[Fe(bpy)_3]^{2+}$ and Z-$[Ru(bpy)_3]^{2+}[Fe(tpy)_2]^{2+}$. The co-doped zeolites were prepared in a similar manner to the iron doped zeolites, except that the Z-$[Ru(bpy)_3]^{2+}$ was employed instead of Na−Y zeolite. The reaction with 2,2′-bipyridine or 2,2′:6′,2″-terpyridine was carried out by refluxing in ethanol. The products were filtered and washed with copious amounts of hot ethanol. The co-doped materials were then dispersed in NaCl (10% w/v, 500 mL) and stirred for 30 min in order to remove superficially surface bound iron species then washed with deionized water until no chloride could be detected using silver nitrate solution (0.1 M). These materials were dispersed in ethanol, warmed, filtered twice, and then extensively washed with ethanol in order to remove excess unreacted ligand.

Results and Discussion

Synthesis and Characterization. To encapsulate $[Ru(bpy)_3]^{2+}$ and $[Fe(L-L)_n]^{2+}$ within the 13 Å supercage of zeolite Y , a ship in a bottle synthesis was employed. Metal precursors and ligand were ion exchanged or diffused into the zeolite and reacted in situ. Once formed, the complexes are physically trapped and cannot leach out of the zeolite since the molecular diameter of the product exceeds the size of the pore entrance. The resulting powders were washed and ion-exchanged extensively to eliminate encapsulated reagent or any surface bound complex. Soxhlet extraction was used to eliminate any unreacted ligand.

TABLE 1: Concentrations of Co-doped Materials

conc $[Fe(bpy)_3]^{2+}$ [a] within Z-$[Ru(bpy)_3]^{2+}$ [b]		total loading[c]	conc $[Fe(tpy)_2]^{2+}$ [a] within Z-$[Ru(bpy)_3]^{2+}$ [b]		total loading[c]
mol dm^{-3}	supercages per $[Fe(bpy)_3]^{2+}$	supercages per $M(LL)_n$	mol dm^{-3}	supercages per $[Fe(tpy)_2]^{2+}$	supercages per $M(LL)_n$
0.0334	26.5	12.1	0.119	7.4	5.6
0.0187	47.4	15.2	0.056	15.8	9.3
0.0162	54.7	15.9	0.038	23.3	11.4
0.0127	69.8	16.9	0.027	32.8	13.3
0.0120	73.8	17.2	0.024	36.9	13.9
0.0090	98.4	18.2	0.019	46.6	15.1
0.0080	110.7	18.6	0.016	55.4	15.9
			0.015	59.1	16.2
			0.0096	92.4	18.0

[a] Based on Y-zeolite with density 1.92 g/cm^{-3} and 1 g Y-zeolite containing 2.778×10^{20} supercages.[53,54] [b] Concentration of Z-$[Ru(bpy)_3]^{2+}$ remained constant at 0.0396 Mol dm^{-3}, corresponding to 1 $[Ru(bpy)_3]^{2+}$ per 22 supercages. [c] Represents combined loading of donor and acceptor complexes.

For the purposes of discussing the loading of metal complexes into zeolite Y, we use the number of supercages per metal complex or percentage occupancy, for example 1 metal complex per 20 supercages, represents a five percent occupancy of zeolite supercages or the concentration is expressed in mol dm^{-3} as described by Dutta et al.[26]

On the basis of the solution-phase extinction coefficient, electronic absorbance spectroscopy, vide infra, indicated that Z-$[Ru(bpy)_3]^{2+}$ contained 1 $[Ru(bpy)_3]^{2+}$ per 22 supercages. This material was subsequently doped with the desired loading of either $[Fe(bpy)_3]^{2+}$ or $[Fe(tpy)_2]^{2+}$ to yield the co-doped materials. A single synthetic batch of Z-$[Ru(bpy)_3]^{2+}$ was used for all iron encapsulation reactions. The concentrations of metal complex within the zeolite was confirmed by dissolving 50 mg of the zeolite material in hydrofluoric acid (1 mL, 10% V/V), and the concentrations of $[Ru(bpy)_3]^{2+}$, $[Fe(bpy)_3]^{2+}$, and $[Fe(tpy)_2]^{2+}$ were then estimated from their visible absorbance.[27] The electronic absorbance was measured in HF solution directly after dissolution. In separate experiments, we confirmed that $[Ru(bpy)_3]^{2+}$, $[Fe(bpy)_3]^{2+}$, and $[Fe(tpy)_2]^{2+}$ were all stable in 10% V/V HF over periods at least twice as long as those required for the zeolite analysis. The concentrations of the co-doped materials are shown in Table 1. In order to ensure that no uncomplexed iron persisted in the zeolite, additional 2,2′-bipyridine and ascorbic acid were added to the extracted supernatant. This did not alter the absorption spectrum, indicating that any uncomplexed iron remaining after reaction had been removed. Separate experiments confirmed that iron polypyridyl complexation occurs in low pH solutions, precluding the possibility that the low pH of the HF solution could affect the quantization of the uncomplexed iron. The diffuse reflectance spectrum of Z-$[Ru(bpy)_3]^{2+}$ shows a weak shoulder at ~545 nm. This is attributed to a small amount of native iron impurity within the native zeolite material, which persisted after purification. This constituted less than 1 iron per 150 supercages.[28]

Spectroscopy. *Diffuse Reflectance Spectroscopy.* Both $[Ru(bpy)_3]^{2+}$ and $[Fe(bpy)_3]^{2+}$ included separately in zeolite Y have been reported and the electronic spectroscopy of our products agreed closely with these reports.[23,29,30,31]

In order to assess if there were any changes to the respective spectra of Z-$[Ru(bpy)_3]^{2+}$ and Z-$[Fe(bpy)_3]^{2+}$ when co-doped, we compared the electronic spectroscopy of the individual complexes in zeolite Y with those in which the metal complexes are combined. Figure 1A shows the diffuse reflectance spectra of approximately 1:20 metal to pore loadings (5% total pore occupation) of (i) Z-$[Ru(bpy)_3]^{2+}$ and (ii) Z-$[Fe(bpy)_3]^{2+}$ in zeolite Y. Figure 1A (iii) shows the linear addition of these

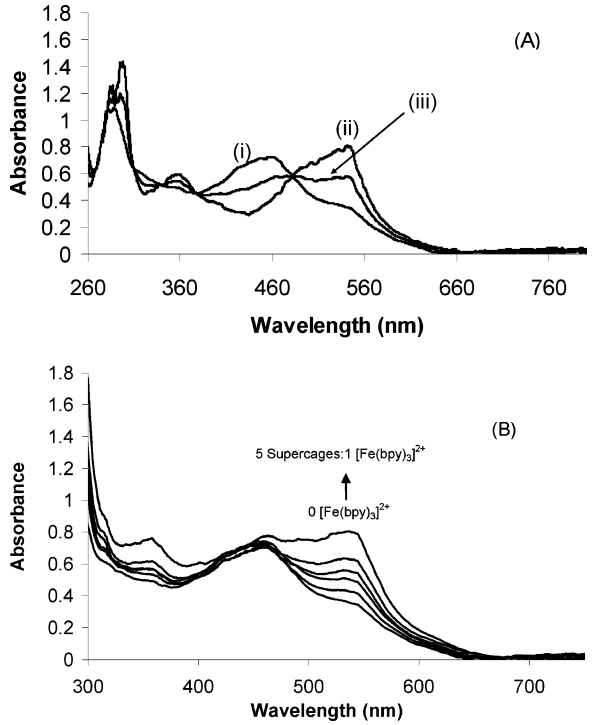

Figure 1. Diffuse reflectance spectra of (i) 1:22 pore Z-$[Ru(bpy)_3]^{2+}$, (ii) 1:20 pore Z-$[Fe(bpy)_3]^{2+}$, and (iii) the averaged combined spectra of the two (b) diffuse reflectance spectra 1:22 Z-$[Ru(bpy)_3]^{2+}$ with increasing concentration of encapsulated Z-$[Fe(bpy)_3]^{2+}$.

two component spectra. Figure 1B shows the diffuse reflectance spectrum of 5% Z-$[Ru(bpy)_3]^{2+}$ with increasing loadings of $[Fe(bpy)_3]^{2+}$. The diffuse reflectance for the co-doped samples show only minor changes to the main MLCT band, where for example there is a slight red shift in the ruthenium absorbance at the highest concentration of $[Fe(bpy)_3]^{2+}$. Overall, however, comparison of the spectrum for 1:22 metal:supercage loadings of Z-$[Ru(bpy)_3]^{2+}$ co-doped with less than 1: 20 metal:supercage loadings of Z-$[Fe(bpy)_3]^{2+}$ shows little evidence for ground state intermolecular interactions between the iron and ruthenium bpy complexes when co-incorporated. Assuming an even distribution of the complexes throughout the zeolite matrix, the probability that adjacent cages contain an ruthenium and iron center is low. For example at the highest loading of $[Fe(bpy)_3]^{2+}$ used here, 1 in 26.5 supercages, the probability of adjacent cages containing a Ru−Fe pair is approximately 14%. Therefore, it is not surprising that electronic spectroscopy indicates no interaction between the co-immobilized complexes.

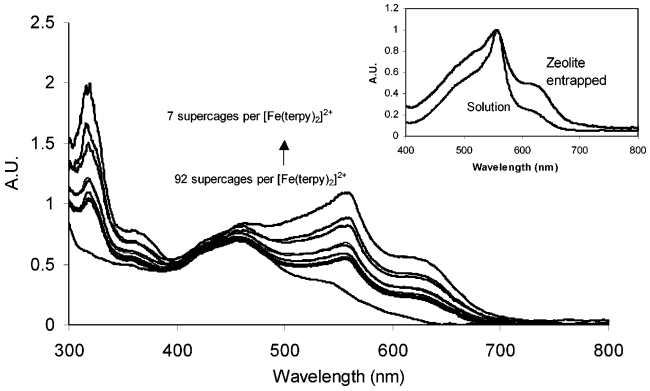

Figure 2. Diffuse reflectance spectra 1:22 pore Z-$[Ru(bpy)_3]^{2+}$ with increasing concentration of encapsulated Z-$[Fe(tpy)_2]^{2+}$, concentrations shown in Table 1. The inset shows the electronic spectrum of $[Fe(tpy)_2]^{2+}$ in DMSO and diffuse reflectance spectrum of $[Fe(tpy)_2]^{2+}$ in zeolite Y 1:20 pore (spectra normalized for comparison purposes).

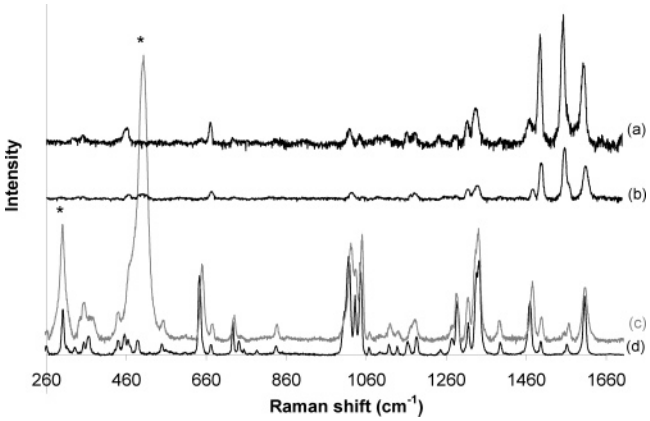

Figure 3. Raman spectroscopy of (a) $[Fe(tpy)_2][PF_6]_2$ powder excited at 458 nm, (b) 1:20 $[Fe(tpy)_2]^{2+}$ encapsulated in zeolite Y, excited at 458 nm, (c) 1:20 $[Fe(tpy)_2]^{2+}$ encapsulated in zeolite Y, excited at 785 nm, and (d) solid $[Fe(tpy)_2][PF_6]_2$ powder excited at 785 nm. * indicates zeolite modes.

Figure 2 shows the diffuse reflectance spectrum of 1:22 loading of Z-$[Ru(bpy)_3]^{2+}$ with increasing loadings of $[Fe(tpy)_2]^{2+}$. The inset compares the diffuse reflectance spectrum of Z-$[Fe(tpy)_2]^{2+}$ (1:20) in the absence of ruthenium and the solution phase absorbance spectrum of $[Fe(tpy)_2][PF_6]_2$ in dimethylsulfoxide (DMSO). In contrast to the co-immobilized bpy system, there is significant broadening of the visible bands of encapsulated $[Fe(tpy)_2]^{2+}$ with concomitant shifts in the absorbance maxima compared to the complex in solution. For $[Fe(tpy)_2]^{2+}$ in DMSO, spectral fitting shows that the $[Fe(tpy)_2]^{2+}$ metal to ligand charge-transfer Fe (t_2g $d\pi$) to terpy (π^*) transition[32] can be deconvoluted into three contributions, centered at 558, 536, and 521 nm.[33] The wavelength of the sharp feature at 558 nm, remains unchanged in zeolite, although its relative intensity is significantly reduced. The features at 536 and 521 nm have been assigned to the Fe (t_2g $d\pi$) to terpy (π^*) transition corresponding to excitation into higher lying levels within the π^* manifold.[32,34] These undergo substantial changes, shifting to 526 nm and 500 respectively upon inclusion in zeolite. In addition, the 526 nm band is considerably broadened and its intensity enhanced in zeolite.

The low-energy tail to the MLCT envelope for $[Fe(tpy)_2]^{2+}$ centered at 625 nm is assigned to an allowed $^1T2 \leftarrow {}^1A1$ ligand field transition.[35] This feature is also strongly influenced by inclusion within the zeolite. This transition is weakly allowed in iron complexes of tridentate imines because the formal octahedral symmetry is reduced toward D_{4h} symmetry. In zeolite, this band is broadened and the relative intensity (as a percentage of the overall visible absorption envelope) of this feature increased by a factor of approximately three. This observation suggests that the deviation away from octahedral geometry increases when encapsulated presumably due to the spatially restrictive zeolite environment. The impact of the zeolite on the geometry of $[Fe(tpy)_2]^{2+}$ complexes is consistent with the very large increases in luminescence intensity and lifetime observed for the analogous ruthenium complex when incorporated in zeolite, although there is some debate as to the origin of the photophysical changes.[36] Such structural changes are furthermore reflected in changes to Raman spectroscopy (vide infra) when $[Fe(tpy)_2]^{2+}$ is encapsulated.

Diffuse reflectance spectra of co-encapsulated $[Ru(bpy)_3]^{2+}$ and $[Fe(tpy)_2]^{2+}$ exhibit MLCT absorptions arising from both guests, the former at 458 nm and the latter at 559 nm, although, like co-doped $[Fe(bpy)_3]^{2+}$ and $[Ru(bpy)_3]^{2+}$ there are no new features to suggest strong ground state communication. At the highest loading of $[Fe(tpy)_2]^{2+}$, the Z-$[Ru(bpy)_3]^{2+}$ MLCT is slightly red-shifted by 4 nm to 462 nm, whereas the Z-$[Fe(tpy)_2]^{2+}$ MLCT formerly at 559 nm undergoes a red shift of 3 nm. These shifts are comparable to those attributed to adjacent cage interactions of $[Ru(bpy)_3]^{2+}$ in zeolite Y and likely to originate from similar inter-cage interactions at high co-loadings.[29]

Raman Spectroscopy. Raman spectroscopy of the doped materials was studied in order to gain insight into structural changes accompanying co-encapsulation. Raman spectroscopy of $[Fe(bpy)_3]^{2+}$ and $[Ru(bpy)_3]^{2+}$ separately encapsulated in zeolite have been reported previously.[37,38]

Figure 3a shows the resonance Raman spectrum of solid $[Fe(tpy)_2][PF_6]_2$ excited at 457.9 nm, and Figure 3b shows the spectrum for Z-$[Fe(tpy)_2]^{2+}$ under the same conditions. This excitation wavelength is pre-resonant with the MLCT transition, and therefore, modes associated with chromophores involved with this transition are enhanced. Comparing the two spectra, it is evident that the zeolite Y framework imposes geometric constraints on $[Fe(tpy)_2]^{2+}$ reflected in spectral shifts. In addition, the Raman features are somewhat broadened in the zeolite attributed to the microenvironmental heterogeneity experienced by individual Z-$[Fe(tpy)_2]^{2+}$ complexes.

Complete normal coordinate analysis have been reported for both $[Fe(tpy)_2]^{2+}$ and the analogous $[Ru(tpy)_2]^{2+}$ complex and these analysis were exploited here in band assignments.[39,40] From Figure 3, panels a and b, there is a general trend toward the higher vibrational frequencies for the complex in zeolite compared with solid or solution.[41] For example, the mode at 671 cm^{-1}, which is assigned to a ring deformation mode, largely confined to the middle terpy ring, is shifted by approximately 4−675 cm^{-1}. The weaker mode, centered at 726 cm^{-1}, attributed to ring deformation modes of the external rings is shifted to a comparable extent. This trend continues for the higher frequency modes between approximately 1450 and 1700 cm^{-1} which possess mostly ring stretch character, where blue shifts of between 5 and 8 cm^{-1} are observed for the zeolite encased complex. Large shifts are observed for the coupled C−H bend ring stretch mode at 1470 cm^{-1} which shifts to 1477 cm^{-1} on encapsulation and the C−H bend at 1163 cm^{-1} shifts to 1177 cm^{-1} in zeolite. The most perturbed mode is the ring stretch at 1245 cm^{-1} which shifts by 16 cm^{-1} to 1261 cm^{-1} in zeolite. The mode at 356 cm^{-1}, which contains mostly Fe−N character, is largely unperturbed by the zeolite matrix. Similar insensitivity in the metal ligand stretch mode toward encapsulation was previously reported for $[Ru(bpy)_3]^{2+}$.[37] We then compared the

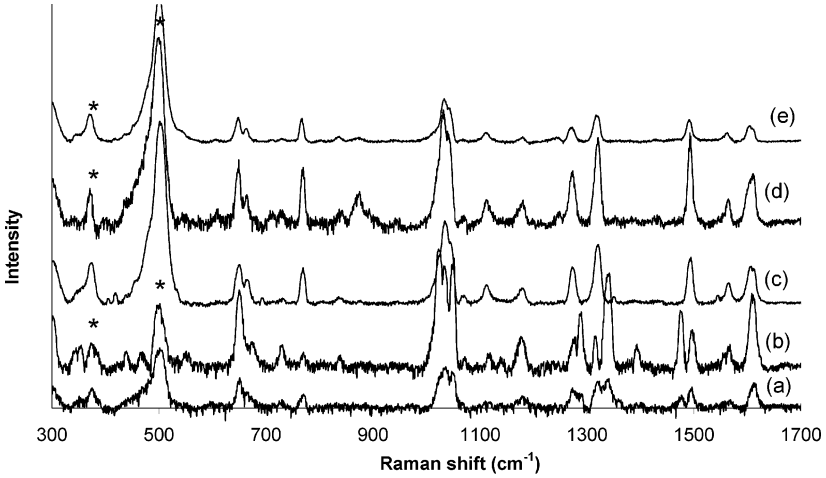

Figure 4. Raman spectroscopy of 1:22 Z-$[Ru(bpy)_3]^{2+}$ doped with (a) $[Fe(tpy)_2]^{2+}$ 1:37 pore, (b) $[Fe(tpy)_2]^{2+}$ in zeolite Y 1:7 pore, (c) $[Fe(bpy)_3]^{2+}$ in zeolite Y 1:74 pore, (d) $[Fe(bpy)_3]^{2+}$ in zeolite Y 1:26 pore, and (e) 1:22 Z-$[Ru(bpy)_3]^{2+}$ alone. $\lambda_{excitation}$ 785 nm. * indicates zeolite modes.

resonant Raman with non-resonant Raman (λ_{ex} 785 nm) spectra of solid and zeolite encapsulated $[Fe(tpy)_2]^{2+}$, and the latter are shown in Figure 3, panels c and d, respectively. Again, there is substantial broadening of many bands, by comparison with solid or solution, but more importantly, significant shifts in certain vibrational modes which were not resonantly enhanced were observed, for example, the ring bend mode at 642.5 cm^{-1} shifts by approximately 8 cm^{-1} to 651 cm^{-1} when the $[Fe(tpy)_2]^{2+}$ is encapsulated. There are, in particular, substantial changes to the cluster of ring stretch modes between 1006 and 1049 cm^{-1}, to the extent that the shoulder at 1006 cm^{-1} and a ring stretch mode at 1248 cm^{-1} in solid $[Fe(tpy)_2]^{2+}$ are lost on encapsulation.[42] A third unassigned feature at 791 cm^{-1} is also lost on encapsulation. Overall, therefore, Raman spectroscopy suggests that the supercage has a significant impact on the on the peripheral structure of the complex consistent with the steric confinement implied by the electronic spectroscopy. Raman spectral shifts of up to 16 cm^{-1} are observed between solid and encapsulated complex and the magnitude of these shifts are considerably greater than those previously reported for $[Ru(bpy)_3]^{2+}$ or $[Fe(bpy)_3]^{2+}$, suggesting greater perturbation to the $[Fe(tpy)_2]^{2+}$ structure. Furthermore, changes to the number of vibrational modes observed may imply changes to the symmetry of the encapsulated complex.

Finally, Figure 4 shows the resonance Raman spectra of the mixed loadings of iron and ruthenium polypyridyl complexes. The Ruthenium content across the materials is constant. The effect of increasing the concentration of iron complex on the ruthenium signature was found to be negligible for most of the materials examined and the Raman spectra are essentially sums of the spectra of the $[Fe(bpy)_3]^{2+}$ or $[Fe(tpy)_2]^{2+}$ and $[Ru(bpy)_3]^{2+}$.

Photophysical Measurements. As reported previously, the Z-$[Ru(bpy)_3]^{2+}$ material exhibits an intense emission at 617 nm with a long-lived excited-state that decays according to biexponential kinetics. Unsurprisingly, neither Z-$[Fe(bpy)_3]^{2+}$ nor Z-$[Fe(tpy)_2]^{2+}$exhibited luminescence under any conditions of temperature or oxygenation explored. For photophysical measurement, we focused on metal loadings up to 1:12 for Z-$[Ru(bpy)_3]^{2+}[Fe(bpy)_3]^{2+}$ and to 1:11 for Z-$[Ru(bpy)_3]^{2+}[Fe(tpy)_2]^{2+}$. The ruthenium concentration remained constant at 1:22 $[Ru(bpy)_3]^{2+}$: supercage throughout. This loading was chosen as it provided sufficient luminescence intensity with relatively low probability of adjacent cage interactions between centers.

Prior to discussing quenching of the encapsulated complexes, it is useful to consider the quenching of $[Ru(bpy)_3]^{2+}$ by $[Fe(tpy)_2]^{2+}$ and $[Fe(bpy)_3]^{2+}$ in solution. The latter was first reported by Creutz et al. where a bimolecular quenching rate constant was reported as 1×10^9 mol s^{-1} in aqueous media which was attributed to a photoinduced energy transfer.[43] Quenching of $[Ru(bpy)_3]^{2+}$ by $[Fe(tpy)_2]^{2+}$ has not been reported. We therefore studied the effect of titrating increasing aliquots of $[Fe(tpy)_2]^{2+}$ into a solution of 5×10^{-5} mol dm^{-3} $[Ru(bpy)_3]^{2+}$.[33] This resulted in a decrease in $[Ru(bpy)_3]^{2+}$ luminescence intensity which was accompanied by distortion of the emission spectral band indicative of radiative energy transfer or trivial quenching of the $[Ru(bpy)_3]^{2+}$ emission. The absence of significant nonradiative energy or electron-transfer quenching was supported by luminescence lifetime studies which confirmed that within experimental error, $[Ru(bpy)_3]^{2+}$ lifetime did not change over the range of $[Fe(tpy)_2]^{2+}$ concentrations investigated.[44]

Z-$[Ru(bpy)_3]^{2+}[Fe(bpy)_3]^{2+}$ and Z-$[Ru(bpy)_3]^{2+}[Fe(tpy)_2]^{2+}$ Emission Spectroscopy. Figure 5, panels a and b, shows that the emission intensity of Z-$[Ru(bpy)_3]^{2+}$ decreases with increasing concentration of both co-entrapped iron complexes. This behavior was anticipated on the basis of the solution-phase studies described above. In the case of $[Fe(bpy)_3]^{2+}$, this was similarly attributed to nonradiative energy transfer. However, the behavior of the $[Fe(tpy)_2]^{2+}$ complex in zeolite contrasted markedly with that in solution where only trivial quenching had been observed. Furthermore, in codoped Z-$[Ru(bpy)_3]^{2+}[Fe(tpy)_2]^{2+}$ over different iron loadings, the distortion to the emission band observed in solution was considerably reduced. In addition, $[Fe(tpy)_2]^{2+}$ elicited a decrease in the Z-$[Ru(bpy)_3]^{2+}$ lifetime whereas mechanically mixing Z-$[Ru(bpy)_3]^{2+}$ and Z-$[Fe(tpy)_2]^{2+}$ resulted in behavior reminiscent of that in solution, vide infra. Indeed, when encapsulated within the zeolite, $[Fe(tpy)_2]^{2+}$ becomes a more efficient quencher of $[Ru(bpy)_3]^{2+}$ excited-state than $[Fe(bpy)_3]^{2+}$. For example, for Z-$[Ru(bpy)_3]^{2+}$ co-encapsulated with 1: 55 $[Fe(tpy)_2]^{2+}$:supercages, the ruthenium luminescence is decreased by approximately 82%, compared with a 52% reduction of emission intensity for a 1:55 loading of $[Fe(bpy)_3]^{2+}$ under identical conditions.

Z-$[Ru(bpy)_3]^{2+}[Fe(bpy)_3]^{2+}$ and Z-$[Ru(bpy)_3]^{2+}[Fe(tpy)_2]^{2+}$ Excited-State Lifetimes. Tables 2 and 3 show the lifetimes of 1:22 Z- $[Ru(bpy)_3]^{2+}$ when co-doped with increasing concentra-

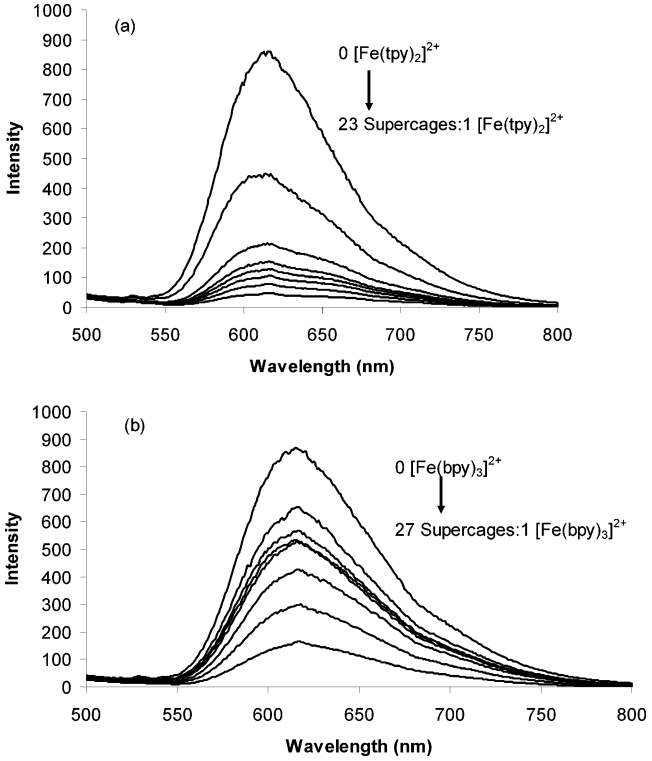

Figure 5. Luminescence spectra of 1:22 Z-$[Ru(bpy)_3]^{2+}$ in the presence of increasing concentrations of co-encapsulated iron polypyridyl complex (a) $[Fe(tpy)_2]^{2+}$ in zeolite Y 1:92, 1:59, 1:55, 1:47, 1:37, 1:33, 1:23, pore, (b) $[Fe(bpy)_3]^{2+}$ in zeolite Y 1:110, 1:98, 1:74, 1:70, 1:55, 1:47, 1:27 pore. Experiments performed in air with $\lambda_{excitation}$ of 452 nm.

TABLE 2: Emission Lifetimes of $[Ru(bpy)_3]^{2+}$ in Zeolite Y with Various Concentrations of Co-encapsulated $[Fe(bpy)_3]^{2+}$

conc $[Fe(bpy)_3]^{2+}$ (mol dm^{-3})[a]	τ_1/ns	A^b	τ_2/ns	B^b
0	771 ± 9	62	390 ± 18	38
0.008	638 ± 5	67	300 ± 3	33
0.009	588 ± 5	70	256 ± 6	30
0.012	616 ± 4	50	308 ± 8	50
0.0127	689 ± 5	35	385 ± 17	65
0.0162	627 ± 5	39	288 ± 11	61
0.0187	555 ± 4	37	236 ± 15	63
0.0334	520 ± 4	23	177 ± 16	77

[a] Concentration of co-encapsulated $[Fe(bpy)_3]^{2+}$ within Z-$[Ru(bpy)_3]^{2+}$ doped zeolite Y. [b] Percent contribution of component lifetime to biexponential decay fit to appropriate exponential model. Lifetimes measured in air equilibrated deionized water.

tions of $[Fe(bpy)_3]^{2+}$ and $[Fe(tpy)_2]^{2+}$ respectively. Figure 6, panels a and b, show plots of Fe loading vs $[Ru(bpy)_3]^{2+}$ lifetime for $[Fe(bpy)_3]^{2+}$ and $[Fe(tpy)_2]^{2+}$, respectively, to highlight trends in the data and the inset shows the effect of increased loading of $[Fe(tpy)_2]^{2+}$ on the luminescent decay of Z- $[Ru(bpy)_3]^{2+}$.

Lifetimes were collected from suspensions of the doped zeolite in air equilibrated deionized water. The water, when filtered, showed no residual emission and the lifetimes recorded were independent of the amount of material suspended. Z-$[Ru(bpy)_3]^{2+}$ alone exhibited a luminescence decay which fitted best to a dual exponential model, to yield τ_1 of 772 ns (69%) and τ_2 of 391 ns (31%). The lifetime of both the short and long components of the Z-$[Ru(bpy)_3]^{2+}$ decay changed on co-inclusion of iron polypyridyl complex.

Crucially, when Z-$[Fe(tpy)_2]^{2+}$ or Z-$[Fe(bpy)_3]^{2+}$ were mechanically mixed with Z-$[Ru(bpy)_3]^{2+}$, the lifetime of Z-$[Ru(bpy)_3]^{2+}$ in the mixture did not change. In the case of the Z-$[Ru(bpy)_3]^{2+}$−Z-$[Fe(tpy)_2]^{2+}$ mixture, decreases in intensity and distortion of emission spectra of Z-$[Ru(bpy)_3]^{2+}$ reminiscent of that observed in solution was observed consistent with radiative energy transfer. However, the reduction in intensity was considerably less than observed for the co-encapsulated complex and as described, there was no significant change in lifetime.[45]

TABLE 3: Emission Lifetimes of $[Ru(bpy)_3]^{2+}$ in Zeolite Y with Varying Concentration of Co-encapsulated $[Fe(tpy)_2]^{2+}$

conc $[Fe(tpy)_2]^{2+}$ (mol dm^{-3})[a]	τ_1/ns	A^b	τ_2/ns	B^b
0	771 ± 9	62	390 ± 18	38
0.0096	653 ± 7	58	153 ± 15	42
0.015	487 ± 6	54	152 ± 11	46
0.016	410 ± 9	45	116 ± 7	55
0.019	386 ± 7	41	109 ± 10	59
0.024	357 ± 13	37	98 ± 41	63
0.027	336 ± 7	29	92 ± 39	17
0.038	308 ± 7	22	77 ± 38	78
0.056	386 ± 3	11	62 ± 3	89
0.119	447 ± 3	16	38 ± 5	84

[a] Concentration of co-encapsulated $[Fe(tpy)_2]^{2+}$ within Z-$[Ru(bpy)_3]^{2+}$ doped zeolite Y. [b] Percent contribution of component lifetime to biexponential decay fit to the appropriate exponential model. Lifetimes measured in air equilibrated deionized water.

Systematic decreases in both lifetime components of Z-$[Ru(bpy)_3]^{2+}$ were observed with increasing Z-$[Fe(bpy)_3]^{2+}$ concentration. For example, the long-lived component decreased from 771 to 505 ns with a loading of 1 $[Fe(bpy)_3]^{2+}$ per 27 supercages and the short-lived component decreased from 390 to 177 ns. The % contribution also changed with increasing loading, the short component dominating at higher iron loadings. For example, for $[Fe(bpy)_3]^{2+}$ at 1 Fe in 27 supercages, the short component represents 77% of the decay contribution.

Interestingly, consistent with the luminescence intensity studies, the impact of Z-$[Fe(tpy)_2]^{2+}$ on the lifetime of Z-$[Ru(bpy)_3]^{2+}$ is greater than for $[Fe(bpy)_3]^{2+}$. Again, a biexponential model adequately fits the decay of Z-$[Ru(bpy)_3]^{2+}$ over the range of $[Fe(tpy)_2]^{2+}$ loadings explored. However, for example, whereas the lifetime of $[Ru(bpy)_3]^{2+}$ decreases to 236 and 555 ns respectively for τ_1 and τ_2, at $[Fe(bpy)_3]^{2+}$ loadings of 1 per 47 supercages, in the presence of equivalent concentrations of Z-$[Fe(tpy)_2]^{2+}$ the decay of $[Ru(bpy)_3]^{2+}$ had reduced to 109 and 386 ns respectively. As Table 3 shows, the lifetimes of $[Fe(tpy)_2]^{2+}$ doped Z-$[Ru(bpy)_3]^{2+}$ material increase at the two highest concentrations of the iron complex. This we attribute to pore blocking of the outer surface of the zeolite particle at the highest iron loadings which prevents penetration of the terpyridine ligands into the zeolite during the iron polypyridyl inclusion reaction. Essentially isolating the $[Ru(bpy)_3]^{2+}$ molecules in the interior of the zeolite particle, from the quencher molecules. Interestingly, whereas the lifetime of $[Ru(bpy)_3]^{2+}$ decreases approximately linearly with Z-$[Fe(bpy)_3]^{2+}$ concentration, it decreases exponentially with $[Fe(tpy)_2]^{2+}$ loading. This is remarkable, given that $[Fe(tpy)_2]^{2+}$ does not quench Z-$[Ru(bpy)_3]^{2+}$ in solution except through trivial/radiative energy transfer, and strongly suggests that a new quenching process occurs in zeolite. Currently, the origin of the difference in loading-lifetime dependence between the two types of iron complex is unclear, but since mechanically mixed Z-$[Fe(tpy)_2]^{2+}$ and Z-$[Ru(bpy)_3]^{2+}$ do not exhibit lifetime changes, it is unlikely to arise simply from a mixture of radiative and nonradiative energy transfer pathways for Z-$[Fe(tpy)_2]^{2+}$.

Nature of Quenching Processes. The luminescent lifetime behavior of Z-$[Ru(bpy)_3]^{2+}$ was reported by Sykora et al., who

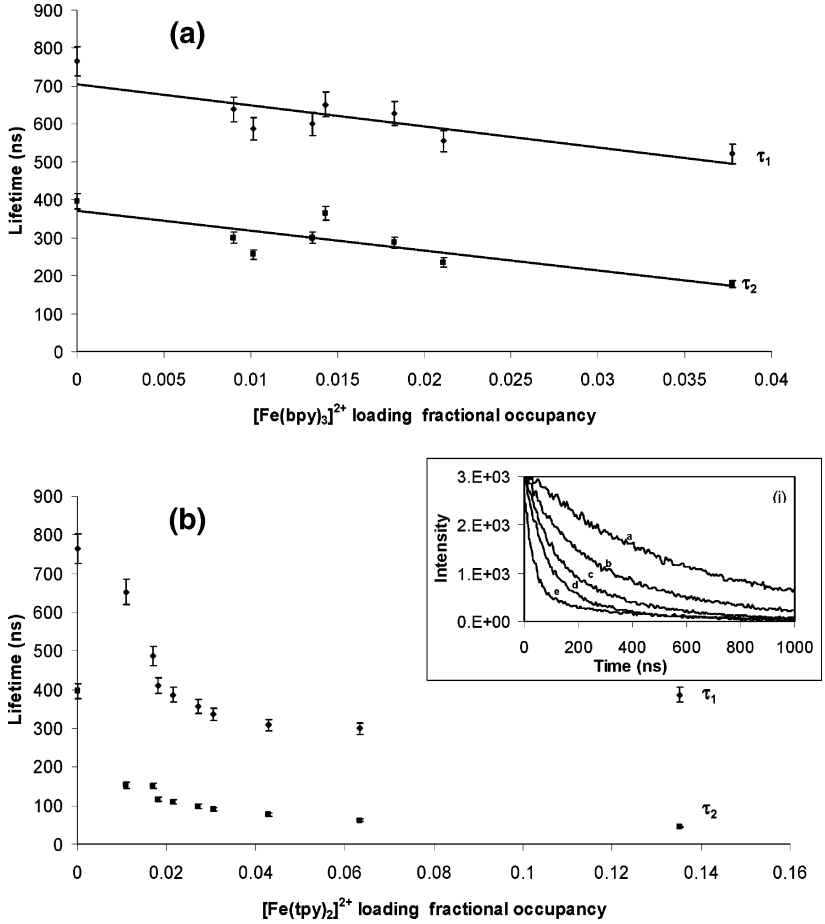

Figure 6. (a) Plots of lifetime of both long (τ_1) and short components (τ_2) of luminescent decay of 1:22 Z-$[Ru(bpy)_3]^{2+}$ versus loading of $[Fe(bpy)_3]^{2+}$. (b) Plots of lifetime of both long (τ_1) and short components (τ_2) of luminescent decay of 1:22 Z-$[Ru(bpy)_3]^{2+}$ versus loading of $[Fe(tpy)_2]^{2+}$. (inset) Luminescent decays for (a) 1:22 Z-$[Ru(bpy)_3]^{2+}$ and 1:22 Z-$[Ru(bpy)_3]^{2+}$ doped with $[Fe(tpy)_2]^{2+}$ at the following pore ratios 1:59 (b), 1:37 (c), 1:23 (d), and 1:7 (e) corresponding to concentrations of entrapped $[Fe(tpy)_2]^{2+}$ of 0.015, 0.024, 0.038, and 0.119 M. Lifetimes recorded in air equilibrated deionized water suspensions.

studied the effect of exciting laser power density and concentration of $[Ru(bpy)_3]^{2+}$ in zeolite Y.[46] Two components of the decay were similarly observed: the long time component was attributed to isolated $[Ru(bpy)_3]^{2+}$ units within the zeolite and the shorter component to adjacent cage interactions originating, potentially from a variety of mechanisms.

The combined concentration of luminophore and quencher in this study was maintained sufficiently low to limit the probability of adjacent cage interactions between two ruthenium's to at most 17% and between a ruthenium and iron to approximately 13% at 1:12 supercages of Iron. A ruthenium-iron adjacent cage interaction at the lowest loading of $[Fe(tpy)_2]^{2+}$ is around 4%, given the significant impact of co-doping on the emission intensity and lifetime even at this loading, this implies that adjacent cage interactions are not required for quenching. This result is consistent with the absorption spectra of the materials which show no significant perturbation of the MLCT or $\pi \rightarrow \pi^*$ transitions of $[Ru(bpy)_3]^{2+}$ except at the highest loading of Z-$[Fe(tpy)_2]^{2+}$. However, we must consider the possibility that the iron quenching behavior is like the self-quenching observed by Sykora et al. for $[Ru(bpy)_3]^{2+}$ at high loadings. Overall, the decrease in luminescence intensity with increasing iron loading observed here is considerably greater than that found for ruthenium self-quenching.[46,29] Any adjacent cage triplet−triplet annihilation within the present system resulting in a short-lived component can be excluded for two reasons. First, time correlated single photon counting was employed for luminescent lifetimes, using a nitrogen discharge lamp whose maximum power would be insufficient to generate two adjacent excited states. Second, the $[Fe(L-L)_n]^{2+}$ complex is unlikely to participate in triplet−triplet annihilation. Electron transfer from $[Fe(bpy)_3]^{2+}$ to $[Ru(bpy)_3]^{2+}$ can be excluded on thermodynamic grounds.[47,48] In addition, electron transfer and Dexter energy transfer, require direct orbital interactions between the donor and acceptor, requiring adjacent cage interactions between $[Fe(bpy)_3]^{2+}$ and $[Ru(bpy)_3]^{2+}$. At low iron loadings, the probability of adjacent cage interactions between $[Ru(bpy)_3]^{2+}$ and $[Fe(L-L)_n]^{2+}$ pairs is not sufficiently high to generate the magnitude of quenching observed. On the basis of Förster energy transfer model, energy transfer between both iron complexes and ruthenium is expected to be exergonic, and likely to be the origin of the quenching.

The Perrin model, eq 1, is commonly applied to excited-state quenching interactions in systems where the donor and acceptor are immobilized, i.e., where no diffusion is possible. The model makes no mechanistic assumptions about the quenching process but proposes a "quenching sphere" centered about the excited molecule. Should a quencher occupy this sphere, the model assumes complete quenching efficiency and zero quenching efficiency outside and assumes a homogeneous distribution of luminophore and quencher within the zeolite

$$\ln(I_0/I) = V_q N_a [Q] \times 10^{-24} \quad (1)$$

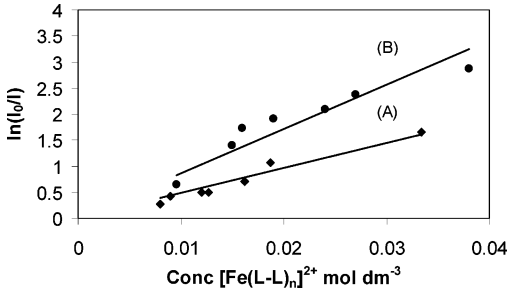

Figure 7. Perrin plots for 1:22 Z-$[Ru(bpy)_3]^{2+}$ quenched by co-encapsulated (A) $[Fe(bpy)_3]^{2+}$ and (B) $[Fe(tpy)_2]^{2+}$. Measurements were performed in air.

where I_0 and I are the luminescence intensity in absence and presence of quencher respectively, V_q the quenching volume, N_a Avogadro's number, and [Q] the quencher concentration.

Figure 7, A and B, shows Perrin plots for quenching of Z-$[Ru(bpy)_3]^{2+}$ by $[Fe(bpy)_3]^{2+}$ and $[Fe(tpy)_2]^{2+}$. Although not shown here, the curves plateau at high iron loadings presumably because inter-cage interactions play a role. The linear portion of the Perrin plots yield quenching sphere radii for the iron terpyridine and iron bipyridine doped samples of 32 and 27 Å, respectively. These values are comparable with the calculated geometrical distances between approximately five and three cages.[46] The important conclusion of the Perrin fit is that the quenching distances substantially exceed that expected for adjacent inter-pore interactions. For example, Dutta et al., applied the Perrin Model to self-quenching occurring in high concentrations of $[Ru(bpy)_3]^{2+}$ in zeolite Y and obtained a quenching radius of 12 Å, leading to the conclusion that adjacent cage interactions were primarily responsible for the luminescence quenching observed. The long-range quenching observed here is consistent with Förster energy, rather than electron, transfer. A significant assumption of the Perrin model is that complete quenching occurs once donor/acceptor lie within the reaction volume whereas the rate of Förster energy transfer varies with donor−acceptor distance.[49,50]

Therefore, the Förster model has been applied. The Förster radius, which is the distance at which energy transfer or spontaneous decay are equally likely can be calculated from the following equation:

$$R_0^6 = \frac{9000(\ln 10)\kappa^2\Phi_D^0}{128\pi^5 N_A n^4}\int_0^\infty I_D(\lambda)\epsilon_A(\lambda)\lambda^4\,d\lambda \qquad (2)$$

where R_0^6 is the Förster radius, κ^2 is the orientational factor which was taken to be 1, Φ_D^0 is the fluorescence quantum yield in the absence of transfer which was taken as 0.042,[51] n is the refractive index of the medium taken to be 1.5,[52] and $\int_0^\infty I_D(\lambda)\epsilon_A(\lambda)\lambda^4\,d\lambda$ is the spectral overlap between donor emission and acceptor absorbance. The spectral overlap was calculated from spectral data for Z-$[Ru(bpy)_3]^{2+}$, $[Fe(bpy)_3]^{2+}$, and $[Fe(tpy)_2]^{2+}$, and found to be 1.3959×10^{-14} and 6.1882×10^{-14} cm^3M^{-1} for the intrazeolitic $[Fe(bpy)_3]^{2+}$ and $[Fe(tpy)_2]^{2+}$ acceptors, respectively. The Förster radii calculated using eq 2 were 22 and 28 Å for Z-$[Ru(bpy)_3]^{2+}$ doped with $[Fe(bpy)_3]^{2+}$ and $[Fe(tpy)_2]^{2+}$, respectively. The apparent switch from trivial energy transfer between $[Ru(bpy)_3]^{2+}$ and $[Fe(tpy)_2]^{2+}$ in solution to nonradiative energy transfer within the zeolite matrix is attributed to enhanced spectral overlap of the donor emission and the acceptor absorption spectra induced by structural distortion of the $[Fe(tpy)_2]^{2+}$ when in the zeolite matrix. As described above, there is a very large increase in absorbance cross section of the low-energy tail of the $[Fe(tpy)_2]^{2+}$ in zeolite Y which represents the acceptor states in a Förster energy transfer.

Conclusions

$[Ru(bpy)_3]^{2+}$ co-encapsulated in zeolite Y with varying concentrations of $[Fe(bpy)_3]^{2+}$ or $[Fe(tpy)_2]^{2+}$ were prepared. The zeolite encased iron complexes were found to quench both intensity and lifetime of the $[Ru(bpy)_3]^{2+}$ complex and this behavior was compared to that found in solution. In solution, $[Fe(bpy)_3]^{2+}$ has been shown to dynamically quench $[Ru(bpy)_3]^{2+}$ through nonradiative energy transfer whereas $[Fe(tpy)_2]^{2+}$ appears to quench only through a radiative or trivial energy transfer mechanism, which exerts no influence on the luminescent lifetime of $[Ru(bpy)_3]^{2+}$. In zeolite, therefore, it appears that for $[Fe(tpy)_2]^{2+}$ the behavior changes and a nonradiative mechanism occurs. The $[Fe(tpy)_2]^{2+}$ exhibits significant structural distortion in the zeolite supercage, which is reflected in Raman and resonance Raman spectroscopy. This reduces the symmetry about the iron coordination sphere, and enhances a $^1T2 \leftarrow ^1A1$ ligand field transition in the complex, enhancing the spectral overlap between $[Ru(bpy)_3]^{2+}$ and $[Fe(tpy)_2]^{2+}$. Therefore, zeolite Y supports and indeed enhances nonradiative energy transfer. The Förster radii were calculated to be 22 and 28 Å for $[Fe(bpy)_3]^{2+}$ and $[Fe(tpy)_2]^{2+}$, respectively, within the zeolite structure, which corresponds to energy transfer across an approximately three cage separation.

Acknowledgment. The authors gratefully acknowledge The Irish Research Council for Science, Engineering and Technology, funded by the National Development Plan for postgraduate scholarship funding under Grant No. RS/2003/103.

Supporting Information Available: Visible absorbance spectra of $[Fe(terpy)_2]^{2+}$, resonance Raman spectrum of $[Fe(tpy)_2]^{2+}$, and solution phase luminescence quenching of $[Ru(bpy)_3]^{2+}$ by $[Fe(tpy)_2]^{2+}$ in acetonitrile. This material is available via the Internet at http://pubs.acs.org.

References and Notes

(1) Walsh, D. A.; Keyes, T. E.; Forster, R. J. *J. Phys. Chem. B* **2004**, *108*, 2631.
(2) Hjelm, J.; Handel, R. W.; Hagfeldt, A.; Constable, E. C.; Housecroft, C. E.; Forster, R. J. *J. Phys. Chem. B* **2003**, *107*, 10431.
(3) Brammer, L. *Chem. Soc. Rev.* **2004**, *33*, 476.
(4) Watton, S. P.; Taylor, C. M.; Kloster, G. M.; Bowman, S. C. *Prog. Inorg. Chem.* **2003**, *51*, 333.
(5) Shughart, E. L.; Ahsan, K.; Detty, M. R.; Bright, F. V. *Anal. Chem.* **2006**, *78*, 3165−3170.
(6) Dutta, P. K.; Ledney, M. *Prog. Inorg. Chem.* **1997**, *44*, 209.
(7) Bruhwiler, D.; Calzaferri, G. *Microporous Mesoporous Mater.* **2004**, *72*, 1.
(8) Diskin-Posner, Y.; Dahal, S.; Goldberg I. *Angew. Chem. Int. Ed.* **2000**, *39*, 1288.
(9) Hashimoto, S. *J. Photochem. Photobiol. C* **2003**, *4*, 19.
(10) Corma, A.; Garcia, H. *Eur. J. Inorg. Chem.* **2004**, *6*, 1143 and references therein.
(11) Borja, M.; Dutta, P. K. *Nature* **1993**, *362*, 43−45
(12) Meier, B.; Werner, T.; Klimant, I.; Wolfbeis, O. S. *Sens. Actuators B* **1995**, *29*, 240.
(13) Krueger, J. S.; Mayer, J. E.; Mallouk, T. E. *J. Am. Chem. Soc* **1988**, *110*, 8232.
(14) Brigham, E. S.; Snowden, P. T.; Kim, Y. I.; Mallouk, T. E. *J. Phys. Chem.* **1993**, *97*, 8650.
(15) Das, S. K.; Dutta, P. K. *Langmuir* **1998**, *14*, 5121.
(16) Coutant, M. A.; Sachleben, J. R.; Dutta, P. K. *J. Phys. Chem. B* **2003**, *107*, 11000.
(17) Sykora, M.; Maruszewski, K.; Treffert-Ziemelis, S. M.; Kincaid, J. R. *J. Am. Chem. Soc* **1998**, *120*, 3490.
(18) Bhuiyan, A. A.; Kincaid, J. R. *Inorg. Chem.* **2001**, *40*, 4464.
(19) Lutkouskaya, K.; Calzaferri, G. *J. Phys. Chem. B* **2006**, *110*, 5633.

(20) Ruiz, A. Z., Li, H. R.; Calzaferri, G. *Angew. Chem.-Int. Ed*. **2006**, *45*, 5282.
(21) Bossart, O.; de Cola, L.; Welter, S.; Calzaferri, *Chem. Eur. J*. **2004**, *10*, 5771.
(22) Bhuiyan, A. A.; Kincaid, J. R. *Inorg. Chem.* **1998**, *37*, 2525.
(23) DeWilde, W.; Peeters, G.; Lunsford, J. H. *J. Phys. Chem*. **1980**, *84*, 2306.
(24) Bossmann, S. H.; Turro, C.; Schnabel, C.; Pokhrel, M. R.; Payawan, L. M.; Baumeister, B.; Wörner, M. *J. Phys. Chem. B* **2001**, *105*, 5374.
(25) $[Fe(bpy)_3][PF_6]_2$ and $[Fe(tpy)_2][PF_6]_2$ was prepared by reaction of ammonium iron(II) sulphate-6-hydrate with the appropriate ligand in hot water and precipitation by addition of aqueous ammonium hexafluorophosphate.
(26) Concentration was calculated taking the density of zeolite Y to be 1.92 g/cm^{-3} and the volume of the unit cell of 15 000 Å^3 as described in ref 45.
(27) Maruszewski, K.; Strommen, D. P.; Handrich, K.; Kincaid, J. R. *Inorg. Chem*. **1991**, *30*, 4579.
(28) Wichterlova, B. *Zeolites* **1981**, *1*, 18.
(29) Turbeville, W.; Robins, D. S.; Dutta, P. K. *J. Phys. Chem.* **1992**, *96*, 5024.
(30) Quayle, W. H.; Peeters, G.; De Roy, G. L.; Vansant, E. F.; Lunsford, J. H. *Inorg. Chem*. **1982**, *21*, 2226.
(31) Bossmann, S. H.; Shahin, N.; Le Thanh, H.; Bonfill, A.; Wörner, M.; Braun, A. M. *Chemphyschem* **2002**, *3*, 401.
(32) Krumholz, P. *Inorg. Chem*. **1965**, *4*, 612.
(33) See supplementary material.
(34) Baggio-Saitovitch, E.; De Paoli, M. A. *Inorg. Chim. Acta* **1978**, *27*, 15.
(35) Spence, T. G.; Trotter, B. T.; Posey, L. A. *J. Phys. Chem. A* **1998**, *102*, 7779.
(36) Bhuiyan, A. A.; Kincaid, J. R. *Inorg. Chem*. **1998**, *37*, 2525.
(37) Dutta, P. K.; Incavo, J. A. *J. Phys. Chem.* **1987**, *91*, 4443.
(38) Incavo, J. A.; Dutta, P. K. *J. Phys. Chem*. **1990**, *94*, 3075.
(39) Jensen, P. W.; Jørgensen, L. B. *J. Mol. Struct.* **1982**, *79*, 87.
(40) Hansen, P. W.; Jensen, P. W. *Spectrochim Acta Part A* **1994**, *50*, 169.
(41) Resonance Raman spectra of the complexes in solid and solution phase showed no noticeable shifts and so comparisons are made interchangeably.
(42) Spectral fitting suggests that this band is lost and not merely shifted; however, this region is very congested and it is difficult to make a definitive assignment.
(43) Creutz, C.; Chou, M.; Netzel, T. L.; Okumura, M.; Sutin, N. *J. Am. Chem. Soc*. **1980**, *102*, 1309.
(44) As there is no reason to believe that these two cationic complexes would associate static quenching could be ruled out.
(45) Approximately 80% greater decrease in intensity for the co-encapsulated $[Fe(tpy)_2]^{2+}$ $[Ru(bpy)_3]^{2+}$ complexes compared with the same relative concentrations in the mechanical mixtures.
(46) Sykora, M.; Kincaid, J. R.; Dutta, P. K.; Castagnola, N. B. *J. Phys. Chem. B* **1999**, *103*, 309.
(47) Constable, E. C.; Thompson, A. M. W. C. *J. Chem. Soc. Dalton Trans.* **1992**, *20*, 2947.
(48) ΔG for electron transfer was estimated from the Rehm Weller expression using the redox potentials for the Iron complexes and excited state redox potentials for $[Ru(bpy)_3]^{2+\cdot}$ For example PET from Z-$[Ru(bpy)_3]^{2+}$ to Z-$[Fe(bpy)_3]^{2+}$ is estimated to be 0.65 eV compared with approx. 0.33 eV for the PET from $[Fe(bpy)_3]^{2+}$ to $[Ru(bpy)_3]^{2+}$. Comparable driving forces are anticipated for Z-$[Fe(tpy)_2]^{2+}$.
(49) Roller, R. S.; Winnik, M. A. *J. Phys. Chem. B* **2005**, *109*, 12261.
(50) Inokuti, M.; Hirayama, F. *J. Chem. Phys*. **1965**, *43*, 1978.
(51) Van Houten, J.; Watts, R. J. *J. Am. Chem. Soc.* **1976**, *98*, 4853.
(52) Suárez, S.; Devaux, A.; Bañuelos, J.; Bossart, O.; Kunzmann, A.; Calzaferri, G. *Adv. Funct. Mater*. **2007**, *17*, 2298.
(53) Breck, D. W. *Zeolite Molecular Sieves: Structure Chemistry and Use*; John Wiley and Sons: New York, 1974.
(54) Weitcamp, J., Karge, H. G., Pfeifer, H., Holderich, W., Eds.; *Zeolites and Related Materials*: *State of the Art*; Elsevier: Amsterdam, 1994.